JJEE
Volume 2, Number 1, 2016
Pages 29-52
Jordan Journal of Electrical Engineering
ISSN (Print): 2409-9600, ISSN (Online): 2409-9619

Polarization Ellipse Technique for Fault Classification and Localization in Distribution Systems with High Renewable Generation Penetration

Qais H. Alsafasfeh[a], Mohammad S. Al-Soud[b]

Department of Electrical Power Engineering and Mechatronics, Tafila Technical University, Tafila, Jordan
[a]e-mail: qsafasfeh@ttu.edu.jo
[b]e-mail: msoud@ttu.edu.jo

Received: November 2, 2015 *Accepted: November 22, 2015*

Abstract— A vital attribute of electrical power network is the continuity of service with a high level of reliability. This motivated many researchers to investigate power systems in an effort to improve reliability by focusing on fault detection and classification. The penetration of renewable energy resources in distribution power systems would affect the traditional fault current level and characteristics. Consequently, traditional protection arrangements developed in distribution utilities are difficult in coordination; and the reclosing scheme would be affected. With rapid developments in distribution system automation, the protection coordination and reclosing scheme based on information exchange for the distribution power system can be realized flexibly. In this paper, a new protective relaying framework to detect, classify and localize faults in an electrical power distribution system with a high level of penetration of renewable energy resources is presented. This work will extract fault unique signatures by using polarization ellipse. During the healthy condition, polarization will have a circular shape with radius equal the rated voltage of the system. However, during the fault condition, polarization will have an ellipse shape and the fault signature will be defined according to the ellipse parameters: major axis, minor axis, ellipticity and orientation angle. The least squares criterion will be used to define ellipse parameters. This system will identify, classify and localize any fault instantaneously.

Keywords— Fault, least squares criterion, polarization ellipse.

I. INTRODUCTION

Power distribution systems which are now served by large power generators and enhanced with more distributed generator (DG) architectures are less restrictive. Fault detection has been a focal point in the research of power systems area since the establishment of electricity transmission and distribution systems. The objective of a power system fault analysis is to provide enough information to understand the reasons leading to the interruption, restoration of the handover of power, and perhaps minimization of future occurrences. The analysis should indeed provide us with an understanding of the network that can lead to producing a set of preventive measures which can be implemented to reduce the likelihood of equipment damage. Circuit breakers and other control elements are designed to help protective relays to take appropriate actions [1]-[2] and minimize the damage and length of interruption. Prompt detection of a fault will have a significant impact on the equipment safety since it will engage the circuit breakers instantaneously before any significant damage occurs. With the recent increase in the number of power system networks within one control center, the behavior and effect of faults have become more complex. As a result, fault impacted area has expanded. Researchers in applied mathematics and signal processing have developed many techniques for the detection and classification of faults in traditional electrical power distribution systems. They used them in conjunction with relaying and protection devices. Recent tools include Artificial Neural Network (ANN) and Wavelets among other powerful pattern recognition and classification tools. ANN based algorithms depend on indentifying the different patterns of system variables using impedance information. The proposed neural

Corresponding author's e-mail: msoud@ttu.edu.jo

network architectures suffer from a large number of training cycles and a high computational burden. Another significant drawback for using ANN is it's inefficient due to the sparse network with the need for large size training data. This adds an additional burden on its computational complexity [3]-[6]. Wavelet transform has been proposed by many to decompose voltage and current waves in an effort to identify a fault. It has been reported that wavelet transform based methods for fault detection are fast and effective analysis methods [7]. Others incorporated wavelet transform with other methods such as Probabilistic Neural Network (PNN), adaptive resonance theory, adaptive neural fuzzy inference system, and support vector machines [8]-[11]. Fuzzy logic was also combined with discrete Fourier transform, adaptive resonance theory, principles of estimation and independent component analysis to enhance performance [11]-[16]. In comparison with ANN, Fuzzy logic systems are subjective and heuristic. They are generally simpler than the wavelet transform or the neural network based techniques. Unfortunately, most of the available tools for fault detection and classification are not efficient and are not investigated for real time implementation [4]. There is a need for new algorithms that have high efficiency, general applicability, and suitability for real time usage especially for power distribution system with high penetration of renewable energy. This research proposes a protection scheme to classify and locate the fault in a distribution network with renewable energy DG penetration.

II. THE POLARIZATION ELLIPSE

A. Definition and Parameters

Rotary-spectrum and polarization analysis are widely used in a number of research areas, including optics, geophysics, meteorology, oceanography and radar [17]. These techniques were originally developed for stationary signals. Their starting point is the Cramér–Loève spectral representation for a complex harmonizable random process. To understand polarization ellipse, we are considering the simplest monochromatic and deterministic case whose real and imaginary parts are given by:

$$E_x(t) = E_{0x}\cos(\omega t + \varphi_x) \tag{1}$$

$$E_y(t) = E_{0y}\cos(\omega t + \varphi_y) \tag{2}$$

The components $E_x(t)$ and $E_y(t)$ give rise to a resultant vector in the transverse *x*-*y* plane. The resultant vector describes a locus of points whose form (equation) is now determined. In order to derive the equation described, (1) and (2) are written as:

$$\frac{E_x(t)}{E_{0x}} = \cos(\omega t)\cos(\varphi_x) - \sin(\omega t)\sin(\varphi_x) \tag{3}$$

$$\frac{E_y(t)}{E_{0y}} = \cos(\omega t)\cos(\varphi_y) - \sin(\omega t)\sin(\varphi_y) \tag{4}$$

Based on straightforward algebra, the following relations can be found:

$$\frac{E_x(t)}{E_{0x}}\sin(\varphi_y)-\frac{E_y(t)}{E_{0y}}\sin(\varphi_x)=\cos(\omega t)\sin(\varphi_y-\varphi_x) \tag{5}$$

$$\frac{E_x(t)}{E_{0x}}\cos(\varphi_y)-\frac{E_y(t)}{E_{0y}}\cos(\varphi_x)=\sin(\omega t)\sin(\varphi_y-\varphi_x) \tag{6}$$

Squaring and adding (5) and (6), the two equations yield:

$$\frac{E_x^2(t)}{E_{0x}^2}+\frac{E_y^2(t)}{E_{0y}^2}-2\frac{E_x(t)E_y(t)}{E_{0x}E_{0y}}\cos(\varphi)=\sin^2(\varphi) \tag{7}$$

where $\varphi=\varphi_y-\varphi_x$.

Equation (7) is recognized as the equation of an ellipse. It shows that at any instant of time the locus of points described by an ellipse is called the polarization ellipse.

As shown in Fig. 1, the ellipse has three major parameters: major axis A_{ma}, minor axis A_{mi}, and a common parameterization which uses the orientation angle ψ. The angle between the major axis of the ellipse and the *x*-axis is as follows [18]:

$$\psi=\tan^{-1}\left(\frac{2E_x(t)E_y(t)}{E_{0x}^2-E_{0y}^2}\cos(\varphi)\right) \tag{8}$$

And the ellipticity (ε), the minor to major axis ratio (also known as the axial ratio) is

$$\varepsilon=\frac{A_{ma}}{A_{mi}} \tag{9}$$

By using Euler's formula for (1) and (2), and substituting in (7), the ellipse can be represented as the sum of positive and negative angular frequency phasors [19]:

$$E(t)=E^+e^{jwt}+E^-e^{-jwt} \tag{10}$$

where

$$E^+=\left|E^+\right|e^{j\varphi^+},\ E^-=\left|E^-\right|e^{j\psi^-},\ A_{ma}=\left\|E^+\right|+\left|E^-\right\|,\ A_{ma}=\left\|E^+\right|-\left|E^-\right\|,\ \psi=\frac{1}{2}\left(\psi^++\psi^-\right)$$

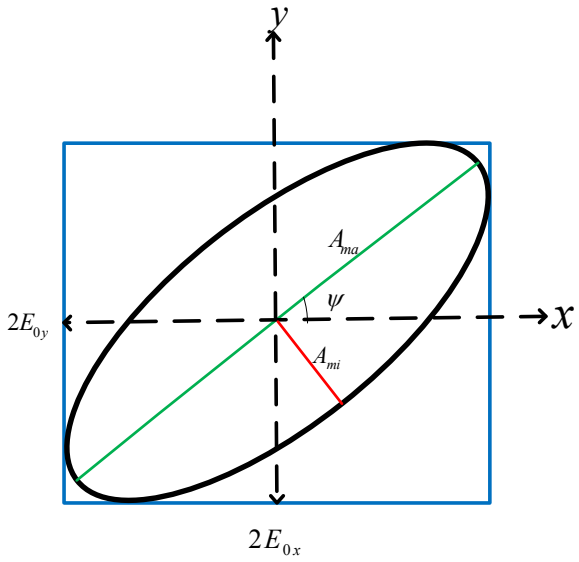

Fig. 1. Polarization ellipse generated from two phasors

B. Degenerate States of the Polarization Ellipse

Three cases are considered here:

- Case 1: the two orthogonal components are in phase. In this case, the ratio of the strengths of the two components is constant. This makes the direction constant. This special case is called linear polarization in which the ellipticity (ε) equals zero.
- Case 2: two orthogonal components have exactly the same amplitude and are exactly ninety degrees out of phase. In this case, one component is zero when the other component is at maximum or minimum amplitude. There are two possible phase relationships that satisfy this requirement: the x component can be ninety degrees ahead of the y component; or it can be ninety degrees behind the y component. So this special case is called circular polarization where the ellipticity (ε) will equal one. This case is used to represent the healthy condition (no fault).
- Case 3: the two components are not in phase and do not have the same amplitude. This kind of polarization is called elliptical polarization because the electric vector traces out an ellipse in the plane (the polarization ellipse). The ellipticity (ε) will be greater than 0 and less than 1. This case will be used to represent the faulty condition. The different types of faults can be verified by using the ellipse parameters (major axis A_{ma}, minor axis A_{mi}, orientation angle (ψ) and ellipticity (ε)) [20].

III. FAULT DETECTION, CLASSIFICATION AND LOCALIZATION BASED ON POLARIZATION ELLIPSE

A. Features Estimation of Fault Signal

We will demonstrate and define parameters based on fault type for simple two-bus power system as shown in Fig. 2, The three phase voltage signal is described by (11). To satisfy ellipse polarization requirement, two orthogonal phasors are needed. To get this condition, we can use Clark's transformation that is described by (12). Traditionally, power systems have been analyzed using symmetrical components, Clark's transformation or any other modal transformation. These polyphase transformations decouple symmetric and cyclic polyphase systems. In balanced power systems or in systems without a neutral return, zero sequence

components are zero. Positive and negative sequences have similar behaviors, especially in symmetric polyphase systems [21].

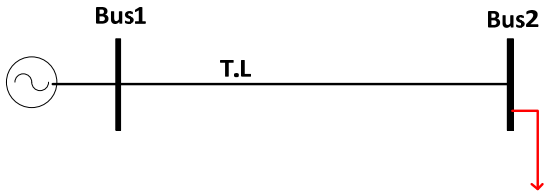

Fig. 2. Simple power distribution system

$$\begin{aligned} V_a(t) &= V_{af}\cos(\omega t-\phi_a)\\ V_b(t) &= V_{bf}\cos(\omega t-\phi_b)\\ V_c(t) &= V_{cf}\cos(\omega t-\phi_c) \end{aligned} \tag{11}$$

$$\begin{pmatrix} x_\alpha(t)\\ x_\beta(t)\\ x_0(t)\end{pmatrix} = \frac{2}{3}\begin{pmatrix} 1 & -\frac{1}{2} & -\frac{1}{2}\\ 0 & \frac{\sqrt{3}}{2} & -\frac{\sqrt{3}}{2}\\ \frac{1}{2} & \frac{1}{2} & \frac{1}{2}\end{pmatrix}\begin{pmatrix} v_a(t)\\ v_b(t)\\ v_c(t)\end{pmatrix} \tag{12}$$

$$x(t)=x_\alpha(t)+jx_\beta(t)=\frac{2}{3}\begin{bmatrix}1 & e^{j\frac{2\pi}{3}} & e^{j\frac{4\pi}{3}}\end{bmatrix}\begin{bmatrix} v_a(t)\\ v_b(t)\\ v_c(t)\end{bmatrix}$$

By using Euler's formula for (11) and substituting in (12), we obtain:

$$\begin{aligned} V_a(t) &= V_{af}\cos(\omega t) &&= \frac{V_{af}}{2}\left(e^{j(\omega t-\phi_a)}+e^{-j(\omega t-\phi_a)}\right)\\ V_b(t) &= V_{bf}\cos(\omega t-\frac{2\pi}{3}) &&= \frac{V_{bf}}{2}\left(e^{j(\omega t-\phi_b)}+e^{-j(\omega t-\phi_b)}\right)\\ V_c(t) &= V_{cf}\cos(\omega t-\frac{4\pi}{3}) &&= \frac{V_{cf}}{2}\left(e^{j(\omega t-\phi_c)}+e^{-j(\omega t-\phi_c)}\right) \end{aligned}$$

(13)

$$\bar{x}=\frac{2}{3}\left[\frac{V_{af}}{2}\left(e^{j(\omega t-\phi_a)}+e^{-j(\omega t-\phi_a)}\right)+e^{j(\frac{2\pi}{3})}\left(\frac{V_{bf}}{2}\left(e^{j(\omega t-\phi_b)}+e^{-j(\omega t-\phi_b)}\right)\right)+e^{j(\frac{4\pi}{3})}\left(\frac{V_{cf}}{2}\left(e^{j(\omega t-\phi_c)}+e^{-j(\omega t-\phi_c)}\right)\right)\right]$$

$$\bar{x}=\frac{1}{3}\left[\left(V_{af}e^{-j\phi_a}+V_{bf}e^{-j\left(\phi_b-\frac{2\pi}{3}\right)}+V_{cf}e^{-j\left(\phi_c-\frac{4\pi}{3}\right)}\right)e^{j(\omega t)}+\left(V_{af}e^{j\phi_a}+V_{bf}e^{j\left(\phi_b+\frac{2\pi}{3}\right)}+V_{cf}e^{j\left(\phi_c+\frac{4\pi}{3}\right)}\right)e^{-j(\omega t)}\right] \tag{14}$$

$$E^+ = \left|E^+\right|e^{j\varphi^+},\ E^- = \left|E^-\right|e^{j\psi^-}$$

$$E^+ = \left(V_{af}e^{-j\phi_a} + V_{bf}e^{-j\left(\phi_b-\frac{2\pi}{3}\right)} + V_{cf}e^{-j\left(\phi_c-\frac{4\pi}{3}\right)}\right)$$

$$\Rightarrow \left|E^+\right| = \frac{1}{3}\sqrt{\left(V_{af}\cos(\phi_a)+V_{bf}\cos\left(\phi_b-\frac{2\pi}{3}\right)+V_{cf}\cos\left(\phi_c-\frac{4\pi}{3}\right)\right)^2+\left(V_{af}\sin(\phi_a)+V_{bf}\sin\left(\phi_b-\frac{2\pi}{3}\right)+V_{cf}\sin\left(\phi_c-\frac{4\pi}{3}\right)\right)^2}$$

$$\angle\psi^+ = \tan^{-1}\left(\frac{-\left(V_{af}\sin(\phi_a)+V_{bf}\sin\left(\phi_b-\frac{2\pi}{3}\right)+V_{cf}\sin\left(\phi_c-\frac{4\pi}{3}\right)\right)}{V_{af}\cos(\phi_a)+V_{bf}\cos\left(\phi_b-\frac{2\pi}{3}\right)+V_{cf}\cos\left(\phi_c-\frac{4\pi}{3}\right)}\right)$$

$$\left|E^-\right| = \frac{1}{3}\sqrt{\left(V_{af}\cos(\phi_a)+V_{bf}\cos\left(\phi_b+\frac{2\pi}{3}\right)+V_{cf}\cos\left(\phi_c+\frac{4\pi}{3}\right)\right)^2+\left(V_{af}\sin(\phi_a)+V_{bf}\sin\left(\phi_b+\frac{2\pi}{3}\right)+V_{cf}\sin\left(\phi_c+\frac{4\pi}{3}\right)\right)^2}$$

$$\angle\psi^- = \tan^{-1}\left(\frac{V_{af}\sin(\phi_a)+V_{bf}\sin\left(\phi_b+\frac{2\pi}{3}\right)+V_{cf}\sin\left(\phi_c+\frac{4\pi}{3}\right)}{V_{af}\cos(\phi_a)+V_{bf}\cos\left(\phi_b+\frac{2\pi}{3}\right)+V_{cf}\cos\left(\phi_c+\frac{4\pi}{3}\right)}\right)$$

For a healthy condition (ideal system):

$$V_{af} = V_{bf} = V_{cf} = V \Rightarrow$$

$$\bar{x} = \frac{2}{3}\left[\left(\frac{3V}{2}\right)e^{j(\omega t)} + \frac{V}{3}\left(1-\frac{1}{2}+j\frac{\sqrt{3}}{2}-\frac{1}{2}-j\frac{\sqrt{3}}{2}\right)e^{-j(\omega t)}\right] = Ve^{j(\omega t)}$$

The trajectory plane will circle with radius equal of rated voltage of the system, but for the fault condition we will examine the trajectory parameter according to the type of fault. Before we start, a number of important points must be clarified [22].

A.1. Single phase to ground Fault

Three different ground faults (AG, BG, and CG) can occur in a power system. To determine the ellipse parameters, we must understand the system behavior during the fault:

- A decrease of voltage (under voltage) in the faulted phase.
- High or low unfaulted voltages, depending on an *X0/X1* equivalent behind the fault. If the ratio *X0/X1* is greater than 1, a higher voltage will occur on the unfaulted phases. For a ratio of three, the overvoltage will reach about 126% of normal values. If the ratio *X0/X1* is less than 1, undervoltage will be experienced on the unfaulted phases. If *X0/X1*, the unfaulted-phase voltages will stay undisturbed with their pre-fault voltage values [23].
- Unfaulted phases are not identical based on phase sequence. As an example for AG fault, the effect on phase *b* is greater than the effect on phase *c* in *abc* sequence.
- At a grounding system or low impedance fault, the voltage difference between faulted and unfaulted phases is high. Voltage difference between unfaulted phases is also high. At an ungrounding system or high impedance fault, voltage difference between faulted and unfaulted phases is low; and voltage difference between unfaulted phases is low.

Now we will set the above condition to define ellipse parameters. There is no phase shift change during the fault $\phi_a = 0$, $\phi_b = 2\pi/3$ and $\phi_c = 4\pi/3$:

A.1.1. Phase A to ground (AG):

$$V_{af} = V_f, V_{bf} = \delta_s V, V_{cf} = V \Rightarrow$$

$$\frac{V_f}{V} \leq \delta_s < 1$$

The orientation angle (ψ) value during AG fault within $\frac{\pi}{3} < \psi \leq \frac{\pi}{2}$ is shown in Fig. 3. The major axis A_{ma} and minor axis A_{mi} at δ_s are:

$$A_{ma} = V, \; A_{mi} = \frac{2V_f + V}{3}$$

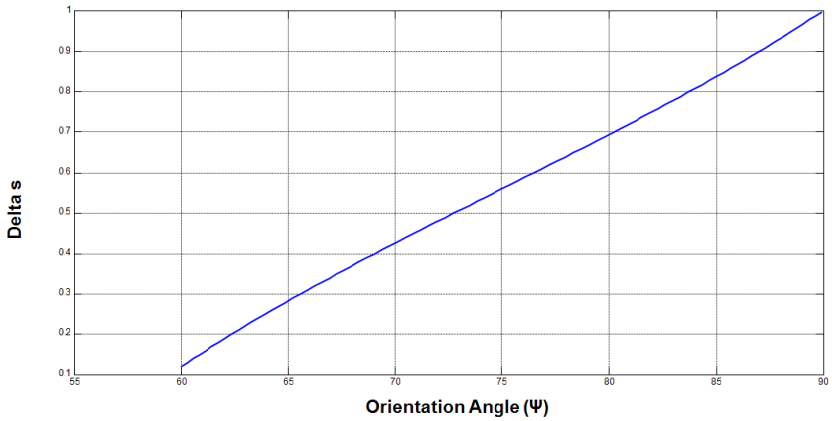

Fig. 3. Orientation angle value during AG fault

A.1.2. Phase B to ground (BG):

$$V_{bf} = V_f, V_{cf} = \delta_s V, V_{af} = V \Rightarrow$$

$$\frac{V_f}{V} \leq \delta_s < 1$$

The orientation angle (ψ) value during BG fault within $0 < \psi \leq \frac{\pi}{6}$ is shown in Fig. 4. The major axis A_{ma} and minor axis A_{mi} at δ_s are:

$$A_{ma} = V, \; A_{mi} = \frac{2V_f + V}{3}$$

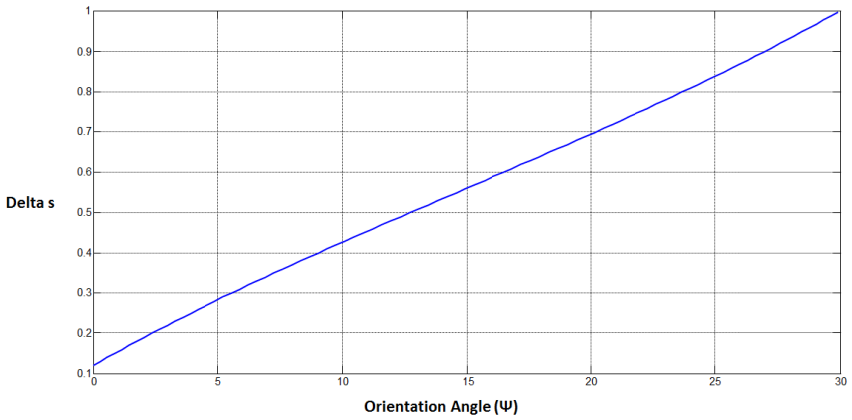

Fig. 4. Orientation angle value during BG fault

A.1.3. Phase C to ground (CG):

$$V_{cf} = V_f, V_{af} = \delta_s V, V_{bf} = V \Rightarrow$$

$$\frac{V_f}{V} \leq \delta_s < 1$$

The orientation angle (ψ) value during CG fault within $\frac{2\pi}{3} < \psi \leq \frac{5\pi}{3}$ is shown in Fig. 5. The major axis A_{ma} and minor axis A_{mi} at δ_s are:

$$A_{ma} = V,\ A_{mi} = \frac{2V_f + V}{3}$$

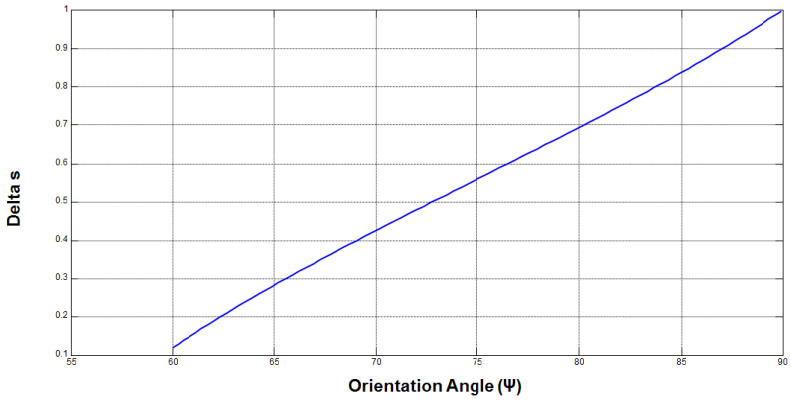

Fig. 5. Orientation angle value during CG fault

In Fig. 6, the blue circle represents the healthy (no fault) condition with a diameter equal to the rated voltage. The red color pattern represents the fault condition with upper limit orientation angles (ψ) $\frac{\pi}{2}, \frac{\pi}{6}$ and $\frac{5\pi}{3}$ for a single phase fault on phase *a*, *b* and *c* respectively. The major axis is equal to the rated voltage.

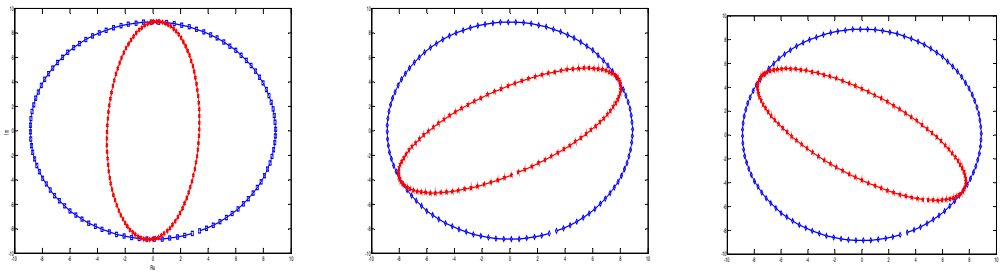

Fig. 6. Polarization ellipse for the single phase to ground faults on phase *a*, *b* and *c* comparing with the circulation ellipse (no fault condition)

A.2. Double phase to ground and phase to phase faults

To determine the ellipse parameters, the system behavior during the fault should be understood:

- A decrease of voltage (undervoltage) in faulted phases.
- About an equal voltage drops in the faulted phases based on phase sequence. As an example for ABG fault, the voltage drop in phase *b* is less than the voltage drop in phase *a* in *abc* sequence.
- The voltage in the healthy phase remains unchanged or increased [23].
- At a grounding system or low impedance fault, the voltage difference between faulted phases is low, and the voltage between faulted and healthy phases is large. Also, for an ungrounded system or a system with high ground impedance, the voltage difference between faulted phases is large; and the voltage difference between faulted and healthy phases is low.

A.2.1. Phase A and B to ground (ABG) and (AB)

$V_{af} = V_f, V_{bf} = \delta_d V_f, V_{cf} = V \Rightarrow$ The orientation angle (ψ) value during ABG fault within $\frac{\pi}{6} < \psi \leq \frac{\pi}{3}$ is shown in Fig. 7, and major axis A_{ma}, minor axis A_{mi} at $\delta_s = 1$ will equal $A_{ma} = \frac{V_f + 2V}{3}$, $A_{mi} = V_f$

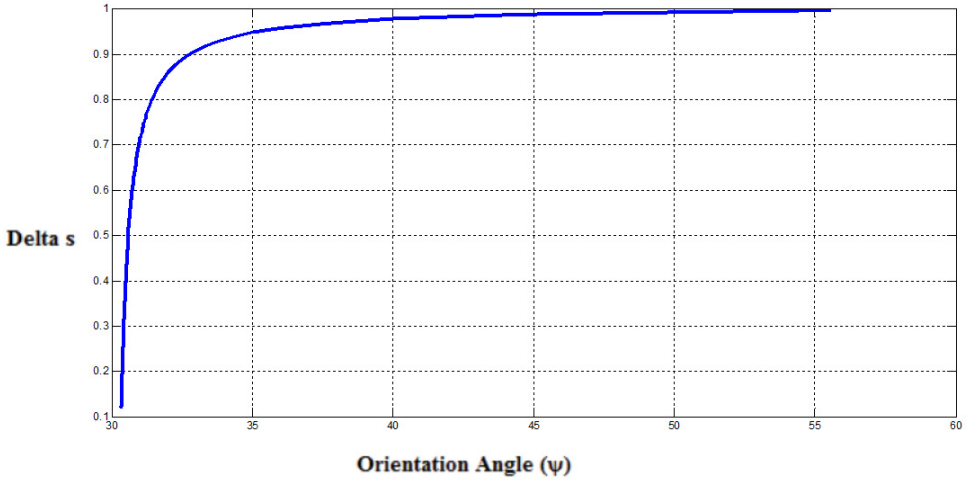

Fig. 7. The orientation angle (ψ) value during CG fault

A.2.2. Phase B and C to ground (BCG) and (BC)

$V_{bf} = V_f, V_{cf} = \delta_d V_f, V_{af} = V \Rightarrow$ The orientation angle (ψ) value during BCG fault within $\frac{5\pi}{3} < \psi \leq \pi$ is shown in Fig. 8, and major axis A_{ma}, minor axis A_{mi} at $\delta_s = 1$ will equal

$$A_{ma} = \frac{V_f + 2V}{3},\ A_{mi} = V_f$$

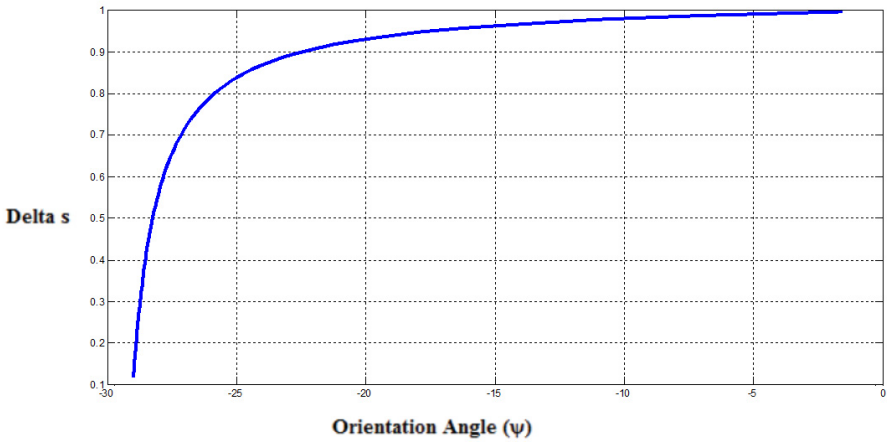

Fig. 8. The orientation angle (ψ) value during CG fault

A.2.3. Phase A and C to ground (ACG) and (AC)

$V_{cf} = V_f, V_{af} = \delta_d V_f, V_{bf} = V \Rightarrow$ The orientation angle (ψ) value during ACG fault within $\frac{\pi}{2} < \psi \leq \frac{3\pi}{2}$ is shown in Fig. 9, and major axis A_{ma}, minor axis A_{mi} at $\delta_s = 1$ will equal

$$A_{ma} = \frac{V_f + 2V}{3},\ A_{mi} = V_f$$

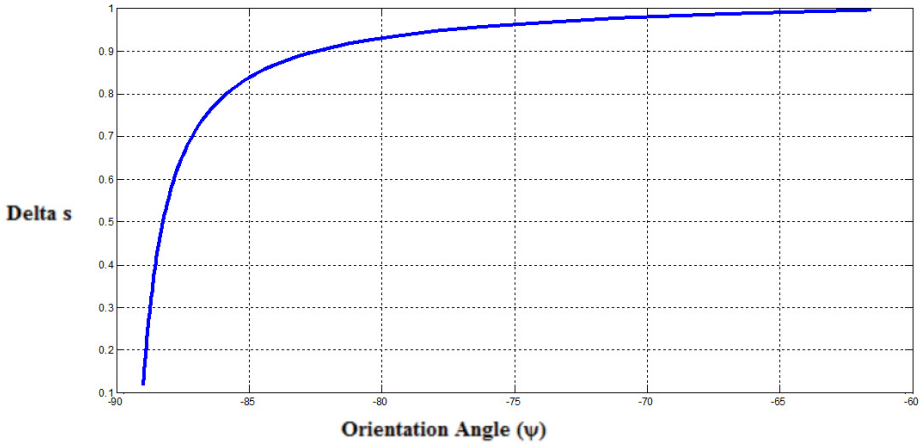

Fig. 9. The orientation angle (ψ) value during CG fault

In Fig. 10, the blue circle represents the healthy (no fault) condition with a diameter equal to the rated voltage; and the red color pattern represents the fault condition with upper limit orientation angles (ψ) are $\frac{\pi}{3}, \pi$ and $\frac{2\pi}{3}$ for double phase to ground fault ABG, BCG and ACG respectively. The major axis is the rated voltage.

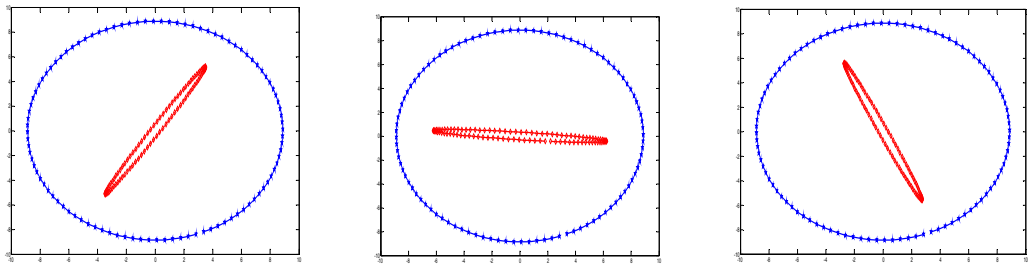

Fig. 10. Polarization ellipse for double phase to ground faults on phase ABG, BCG and ACG compared with the circulation ellipse (no fault condition)

In Fig. 11, the blue circle represents the healthy (no fault) condition with a diameter equal to the rated voltage; and the red color pattern represents the fault condition with upper limit orientation angles (ψ) are $\frac{\pi}{3}, \pi$ and $\frac{2\pi}{3}$ for double phase fault AB, BC and AC respectively. These values have the same orientation angles value for double phase to ground fault. The major axis is greater than or equals the rated voltage because the non-faulted phase does not change. In the grounded fault, the non faulted phase will however change.

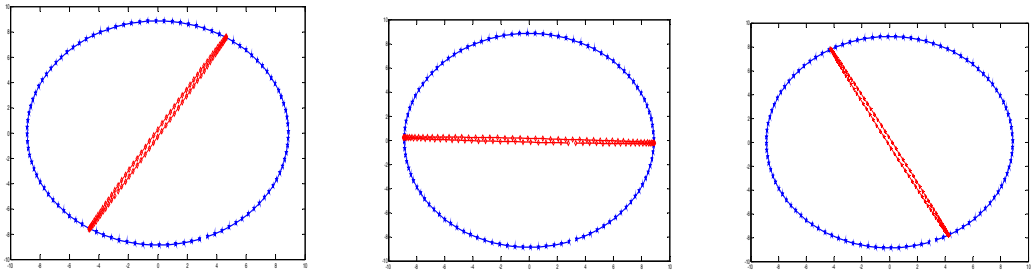

Fig. 11. Polarization ellipse for phase to phase faults on phase AB, BC and AC compared with the circulation ellipse (no fault condition)

In Fig. 12, the blue circle represents the healthy (no fault) condition with a diameter equal to the rated voltage. The red circle represents the fault condition for a symmetrical fault with a diameter equal to the voltage fault.

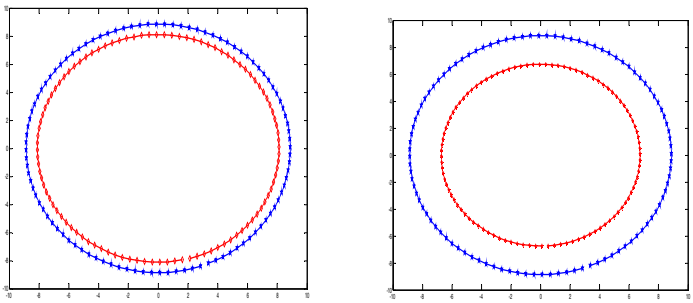

Fig. 12. Polarization ellipse for a symmetrical fault compared with the circulation ellipse (no fault condition)

Table 1 and Fig. 13 show that the nine types of asymmetric fault can be distinguished by the orientation angle easily. The double phase to ground and double phase can be distinguished using the major axis. The angle will change based on the fault resistance. The upper limit angle will start at a very low fault impedance and reach the lower limit for very high fault impedance. The end limit with maximum $\frac{\pi}{6}$ for many buses system orientation angles will be maximum at faulted bus because the minimum voltage at faulted bus and the value of orientation angles will decrease. For symmetrical faults:

$$V_{af} = V_{cf} = V_{bf} = V_f \Rightarrow$$
$$A_{ma} = V_f,\ A_{mi} = V_f$$

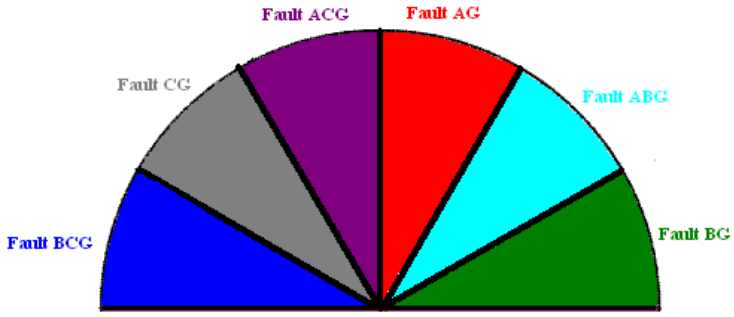

Fig. 13. Fault feature based on ellipse orientation angle

TABLE 1
FAULT FEATURE BASED ON POLARIZATION ELLIPSE

Fault Type	Ψ	A_{ma}	A_{mi}
AG	$\frac{\pi}{3} < \psi \le \frac{\pi}{2}$	V	$\frac{2V_f + V}{3}$
BG	$0 < \psi \le \frac{\pi}{6}$	V	$\frac{2V_f + V}{3}$
CG	$\frac{2\pi}{3} < \psi \le \frac{5\pi}{3}$	V	$\frac{2V_f + V}{3}$
ABG	$\frac{\pi}{6} < \psi \le \frac{\pi}{3}$	$\frac{V_f + 2V}{3}$	V_f
ACG	$\frac{\pi}{2} < \psi \le \frac{3\pi}{2}$	$\frac{V_f + 2V}{3}$	V_f
BCG	$\frac{5\pi}{3} < \psi \le \pi$	$\frac{V_f + 2V}{3}$	V_f
AB	$\frac{\pi}{6} < \psi \le \frac{\pi}{3}$	V	V_f
AC	$\frac{\pi}{2} < \psi \le \frac{3\pi}{2}$	V	V_f
BC	$\frac{5\pi}{3} < \psi \le \pi$	V	V_f
ABC	-	V_f	V_f

B. Fault Incident Point

The fault incident point can be found by performing a cycle-by-cycle comparison around the triggering time. When no match exists between the present and preceding (one cycle ago) cycles, the point at which an over- or undercurrent or voltage can be designated as the fault incident point (time= 0 point or reference point) [23].
The above algorithm can be applied on one cycle of the fault incident point to ensure the generated fault feature based on ellipse parameters. Each cycle contains 80% fault signal after fault incident point. For example, if we have a single line to ground fault AG as shown in (15), the algorithm can ensure fault feature based on ellipse parameters if $t_f < \pi/2$.

$$
\begin{aligned}
Va(t) &= \begin{cases} V\cos(\omega t) & 0 \le t < t_f \\ 0.2V\cos(\omega t) & t_f \le t < 2\pi \end{cases} \\
Vb(t) &= V\cos(\omega t - \frac{2\pi}{3}) \;\; 0 \le t < 2\pi \\
Vc(t) &= V\cos(\omega t - \frac{4\pi}{3}) \;\; 0 \le t < 2\pi
\end{aligned}
\tag{15}
$$

IV. FAULT DETECTION, CLASSIFICATION AND LOCALIZATION ALGORITHM

A. Fault Detection

The polarization methodology is divided into three steps. The first step captures the voltage signal during the first cycle. In the second step, Clark's transformation is applied to generate α and β components by reducing the fault signal from three signals to two perpendicular signals. The polarization ellipse can be applied by using least squares criteria. The ellipse parameters were estimated. From ellipticity (ε), we can decide whether this signal is faulted or not. For the healthy signal, the ellipticity value will equal one; and for faulted signal, the ellipticity value will be less than one. In a real system, the values of all phases in the healthy system are not identical. According to IEEE distribution standards, the difference between all phases must not exceed ±2%. Referring to (13), we assume $V_a = V$, $V_b = \delta V$ and $V_c = \delta V$, where δ is the percentage change in value during the healthy condition according to IEEE for fault detection δ equal 0.98:

$$
\bar{x} = \frac{V}{3}(1+2\delta)e^{j(\omega t)} + \frac{V}{3}(1-\delta)e^{-j(\omega t)}
$$

$$
A_{ma} = \frac{V}{3}(2+\delta),\; A_{mi} = \delta V, \varepsilon = \frac{3\delta}{2+\delta}
$$

At δ equal 0.98, the ellipticity value will equal 0.9866. According to this standard, if ellipticity value is greater than 0.9866, the signal will be of a healthy condition. If ellipticity value is less than 0.9866, it will be a faulted signal.

B. Fault Localization

The algorithm can detect if the system has fault or not. For many buses system, the voltage drop during fault will be maximum at faulted bus; and the value will be decreased in the

direction of the source. The orientation angles are inversely prepositional with voltage magnitude, so the fault location can be easily detected at the maximum value of orientation angles.

C. Fault Classification

After localizing the faulted bus, the fault classification step will be started. The value of the orientation angles is considered according to Table 2. Non-symmetrical fault can be easily identified by the orientation angle. Double phase to ground and double phase faults can be distinguished using the major axis feature. Flow chart shown in Fig. 14 represents the algorithm fault detection, classification and localization.

V. CASE STUDY

The radial network consists of 8km length of 11kV feeder. Although there are more than 19 nos. of distribution transformer centers (DTC) of various ratings, transformers of lower ratings have been lumped with their equivalent ratings being considered for the study without changing the characteristics of the loads.

- Ratings of transformers are 250kVA, 500kVA and 1000kVA respectively.
- The utility substation is represented as a 11kV source with its equivalent power frequency short circuit capacity of 750MVA.

The electrical part of DG1 is represented by a synchronous generator connected to the utility grid. The mechanical systems (wind source component, wind turbine component and wind governor of the DG1) are also modeled. This case shows a synchronous generator being driven by a wind turbine. The turbine is controlled by a wind governor. The wind source is used to model wind speed fluctuations. The rated power is 2MVA; and the rated voltage is 11kV. The wind regenerator is connected to bus 9. The electrical part of DG2 is represented by a solar system connected to the utility grid. The rated power is 250kW; and the rated voltage is 11kV. The solar system is connected to bus 4 as depicted in Fig. 15.

A. Distributed Generation Impact on Smart Grid

A high penetration of distributed generation (DG) may influence the operation and control of the distribution system and the transmission system, leading to technical issues that must be identified and analyzed. The distributed generators are small or medium scale units connected to the low or medium voltage networks (LV or MV). So before starting to apply the fault detection algorithm, we need to verify that the proposed distribution system simulation model can operate in different modes with high DER penetration. Distribution generator impacts will be studied and its performance and operational scenarios will be analyzed:

- Case 1: Steady state voltage profiles have been evaluated using a load flow method to check the voltage pattern and possibility of overloading.
- Case 2: Transient stability analysis was performed particularly when faults occur in the system.

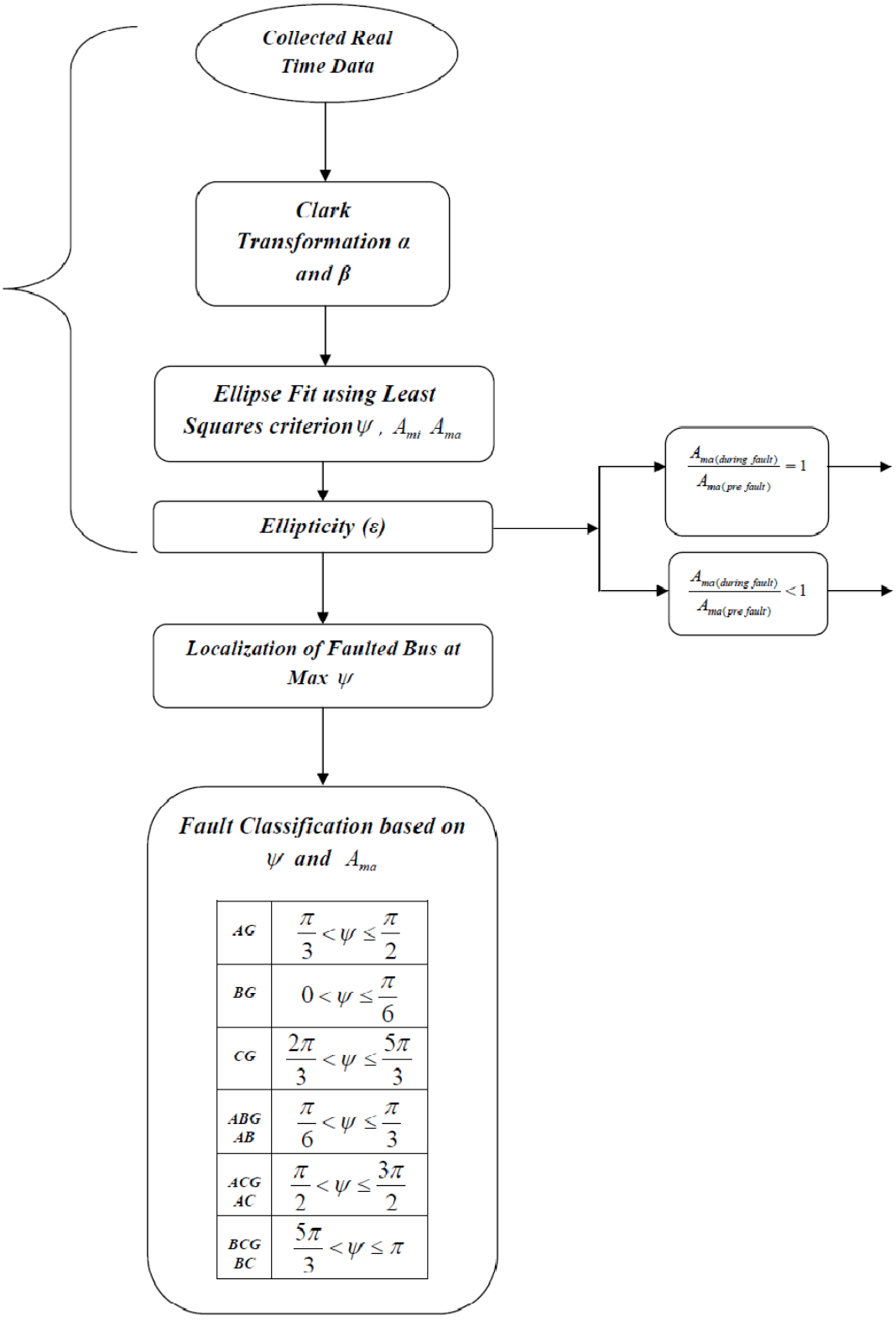

Fig. 14. Polarization ellipse algorithm for fault detection, classification and localization

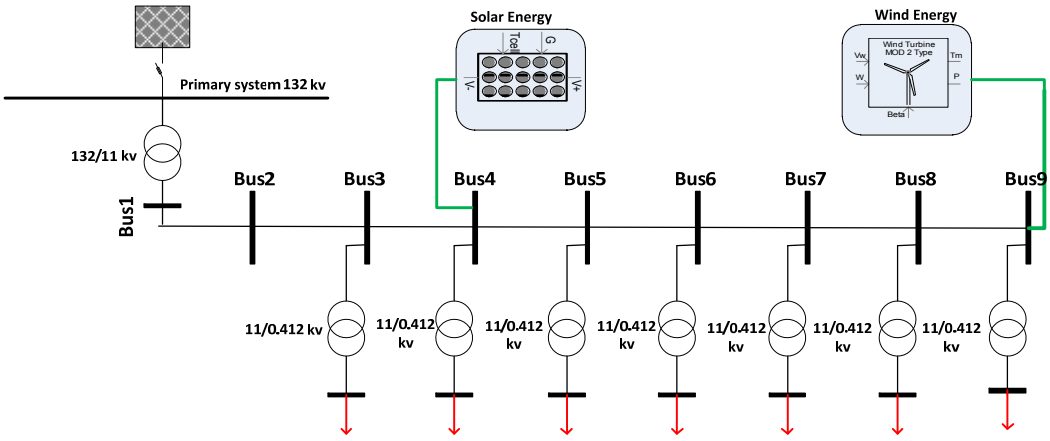

Fig. 15. Smart grid network

A.1. Steady state analysis

One of the main benefits of integration of distributed generation to electricity networks is the improvement of the steady state voltage profile of the system. The result of steady state voltage profile obtained for all buses after employing DG I and DG II is presented in Table 2 which shows the simulation results for four cases without RER Integration, with Wind Integration, with Solar Integration and with wind & Solar Integration. Table 2 also shows that a voltage deviation in Smart Grid still occurs due to imbalances in active and reactive power generated by the DGs during integration. However, large violations of voltages are not evident on all buses. The overall voltage remains within the allowable range and the wind energy source and the solar energy source work as expected.

TABLE 2
OVERALL SMART GRID VOLTAGE, ACTIVE AND REACTIVE POWER PROFILE AFTER EMPLOYING DG I AND DG II

Bus #	without RER Integration			with Wind Integration			with Solar Integration			with wind & Solar Integration		
	Voltage (kV)	Active Power (kW)	Reactive Power (kVAR)	Voltage (kV)	Active Power (kW)	Reactive Power (kVAR)	Voltage (kV)	Active Power (kW)	Reactive Power (kVAR)	Voltage (kV)	Active Power (kW)	Reactive Power (kVAR)
1	10.83	2.483	1.469	10.76	1.156	2.410	10.83	2.273	1.474	10.76	0.9223	2.476
2	10.75	2.465	1.457	10.70	1.141	2.408	10.75	2.245	1.464	10.70	0.9066	2.466
3	10.70	2.451	1.448	10.65	1.129	2.400	10.70	2.244	1.456	10.66	0.8945	2.458
4	10.61	2.252	1.335	10.58	0.9334	2.290	10.61	2.048	1.346	10.59	0.6991	2.348
5	10.59	1.939	1.137	10.56	0.6205	2.094	10.59	1.948	1.136	10.58	0.6115	2.149
6	10.53	1.753	1.032	10.52	0.2394	1.989	10.53	1.762	1.033	10.53	0.4244	2.044
7	10.28	1.560	0.9132	10.36	0.2394	1.869	10.28	1.569	0.952	10.37	0.2265	1.921
8	10.15	0.8859	0.5335	10.30	-0.459	1.473	10.15	0.8906	0.5354	10.31	-0.476	1.523
9	10.07	0.5572	0.3491	10.30	-0.814	1.271	10.07	0.5602	0.3504	10.30	-0.836	1.319

A.2. Transient stability analysis

The smart grid response following the integration of distributed generation to the network steady state profile has been examined. It demonstrates that the Smart Grid steady state voltage profile is within acceptable limits. We note the voltage profile will be enhanced by renewable energy penetration. Nevertheless, this condition cannot guarantee that the system remains stable if a fault occurs in the system.

The 0.1s self-clearing three-phase fault with 10Ω fault resistance was applied at 1.6s in the middle of transmission line at bus 5. The Smart Grid performance during this symmetrical fault is shown in Fig. 16. During the fault, voltage decreased from 10.95 to 10.17kV for utility source as shown in Fig. 15, 10.84 to 8.39kV for DGI (solar source), 11 to 8.61kV for DGII

(wind source). The smart grid voltage recovers within 0.2s after the clearance of the fault. The system now becomes stable.

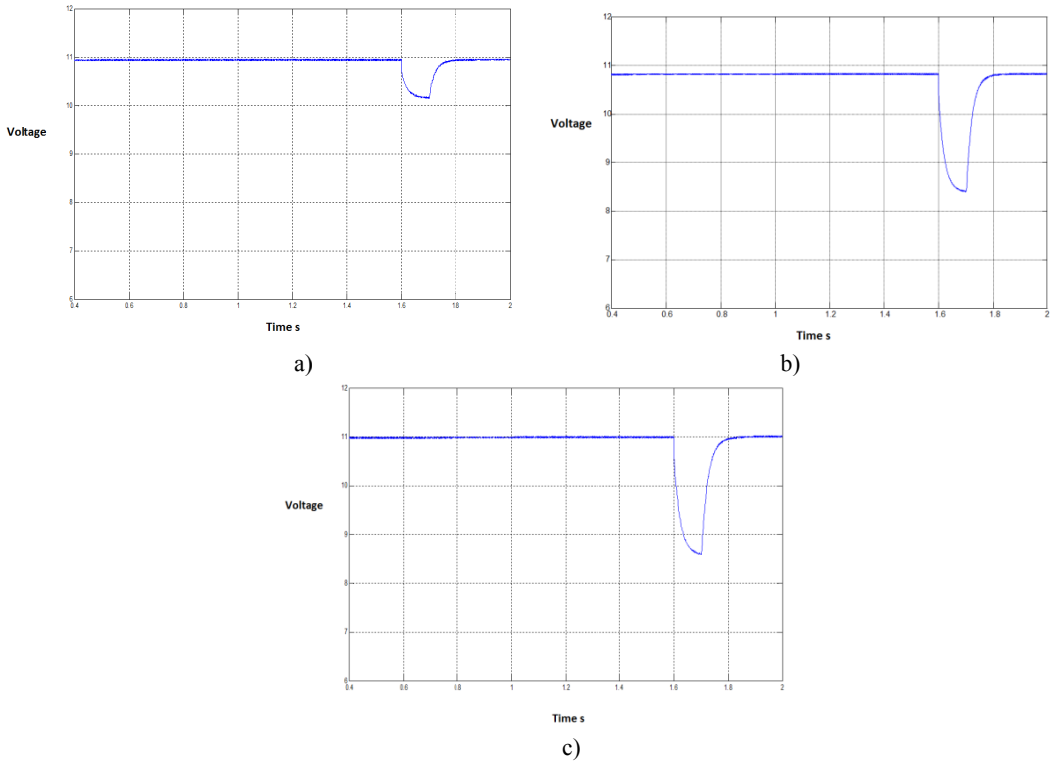

Fig. 16. Voltage (in kV) behavior during three-phase fault, a) at utility bus, b) solar bus and c) wind bus

B. Fault Diagnosis and Localization

The distribution system shown in Fig. 15 was simulated and the previous algorithm was implemented using PSCAD. After applying fault detection, classification and localization algorithm using polarization ellipse, MATLAB software was compared to PSCAD simulations to validate the proposed method

B.1. Single phase to ground fault

The recorded voltage signal of all phases for the single phase to ground fault (AG) was shown in Fig. 17. The first cycle of fault is shown in Fig. 18. After applying Clark's Transformation, α and β component will be extracted using least squares criterion. The ellipse parameter at all buses for AG fault at bus 4 and bus 6 is shown in Table 3 and 4. The ellipticity (ε) at all buses is less than threshold value 0.9866. This means there is a fault in the system. Fault location can be set by looking for the maximum value of ellipse orientation angle ψ. Table 3 shows the maximum value at bus 4; and Table 2 shows the maximum value at bus 6 for both values of fault impedance. The last step classifies type of fault by looking for ψ value. The classification of the fault type is shown in Table 1 and 2. The angle value within $\frac{\pi}{3} < \psi \leq \frac{\pi}{2}$ is based on the fault feature in Table 1. This value indicated fault AG. The same result for BG and CG fault is shown in Table 5 and 6.

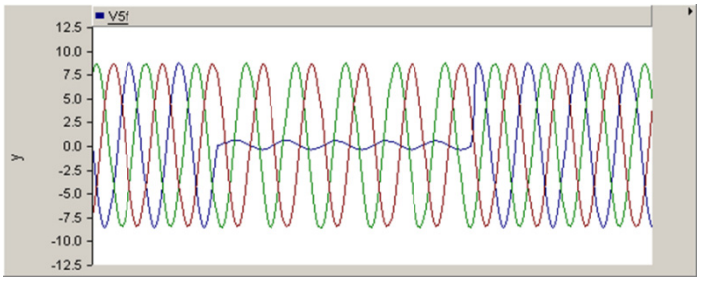

Fig. 17. The recorded voltage signals (in kV) for all phases in case of single phase to ground fault (AG)

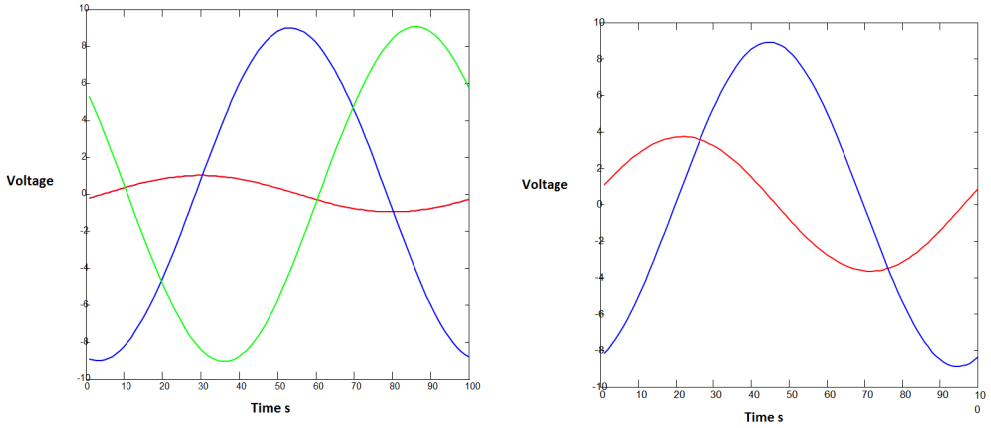

a) b)

Fig. 18. a) Fault voltage signals (in kV) during one cycle, b) Clark's Transformation to α and β components

TABLE 3
ELLIPSE PARAMETER RESULT FOR FAULT AG AT BUS 4

Bus #1			Bus #2			Bus #3			
ψ	A_{ma}	A_{mi}	ψ	A_{ma}	A_{mi}	ψ	A_{ma}	A_{mi}	R_f
74.6433	9.1589	5.9491	80.4946	9.0307	5.0940	83.8256	8.9675	4.4056	0.1
49.9575	8.9608	8.9499	55.1821	8.9310	8.9176	57.9878	8.9082	8.8927	500
Bus #4			Bus #5			Bus #6			
ψ	A_{ma}	A_{mi}	ψ	A_{ma}	A_{mi}	ψ	A_{ma}	A_{mi}	R_f
87.7276	8.9150	3.3317	87.5530	8.9134	3.3549	87.0754	8.9147	3.4219	0.1
61.0621	8.8794	8.8605	60.8659	8.8734	8.8546	60.5220	8.8622	8.8436	500
Bus #7			Bus #8			Bus #9			
ψ	A_{ma}	A_{mi}	ψ	A_{ma}	A_{mi}	ψ	A_{ma}	A_{mi}	R_f
84.9439	8.9440	3.7175	83.0278	9.0603	4.0333	80.7615	9.2324	4.3749	0.1
58.9564	8.8349	8.8173	57.4942	8.8943	8.8773	55.7360	8.9981	8.9817	500

TABLE 4
ELLIPSE PARAMETER RESULT FOR FAULT AG AT BUS 6

Bus #1			Bus #2			Bus #3			
ψ	A_{ma}	A_{mi}	ψ	A_{ma}	A_{mi}	ψ	A_{ma}	A_{mi}	R_f
72.6670	9.1708	6.5708	78.2603	9.0546	5.8673	81.3684	8.9925	5.3006	0.1
49.7359	8.9607	8.9500	54.9368	8.9310	8.9179	57.7295	8.9082	8.8930	500
Bus #4			Bus #5			Bus #6			
ψ	A_{ma}	A_{mi}	ψ	A_{ma}	A_{mi}	ψ	A_{ma}	A_{mi}	R_f
84.8721	8.9313	4.4163	85.8245	8.9196	4.1320	87.9739	8.9042	3.3396	0.1
			61.4827	8.8734	8.8538	63.1115	8.8624	8.8396	500
Bus #7			Bus #8			Bus #9			
ψ	A_{ma}	A_{mi}	ψ	A_{ma}	A_{mi}	ψ	A_{ma}	A_{mi}	R_f
85.8138	8.9331	3.6377	83.8728	9.0493	3.9557	81.5805	9.2210	4.2991	0.1
61.5453	8.8352	8.8135	60.0826	8.8946	8.8737	58.3237	8.9985	8.9783	500

TABLE 5
ELLIPSE PARAMETER RESULT FOR FAULT BG AT BUS 4

Bus #1			Bus #2			Bus #3			
ψ	A_{ma}	A_{mi}	ψ	A_{ma}	A_{mi}	ψ	A_{ma}	A_{mi}	R_f
14.6822	9.1580	5.9427	20.5518	9.0300	5.0882	23.8862	8.9668	4.4005	0.1
-10.105	8.9604	8.9502	-4.8060	8.9309	8.9177	-1.9647	8.9082	8.8927	500
Bus #4			Bus #5			Bus #6			
ψ	A_{ma}	A_{mi}	ψ	A_{ma}	A_{mi}	ψ	A_{ma}	A_{mi}	R_f
27.7825	8.9141	3.3277	27.6104	8.9123	3.3500	27.1411	8.9131	3.4145	0.1
1.0714	8.8794	8.8605	0.9464	8.8734	8.8546	0.6028	8.8622	8.8436	500
Bus #7			Bus #8			Bus #9			
ψ	A_{ma}	A_{mi}	ψ	A_{ma}	A_{mi}	ψ	A_{ma}	A_{mi}	R_f
25.0516	8.9406	3.6996	23.2017	9.0558	4.0065	20.9915	9.2270	4.3382	0.1
-0.9694	8.8350	8.8172	-2.4279	8.8943	8.8773	-4.2174	8.9980	8.9817	500

TABLE 6
ELLIPSE PARAMETER RESULT FOR FAULT CG AT BUS 4

Bus #1			Bus #2			Bus #3			
ψ	A_{ma}	A_{mi}	ψ	A_{ma}	A_{mi}	ψ	A_{ma}	A_{mi}	R_f
134.6645	9.1559	5.9485	140.5959	9.0280	5.0933	143.9251	8.9649	4.4049	0.1
109.9003	8.9608	109.9786	115.2070	8.9176	8.9310	118.0528	8.8927	8.9082	500
Bus #4			Bus #5			Bus #6			
ψ	A_{ma}	A_{mi}	ψ	A_{ma}	A_{mi}	ψ	A_{ma}	A_{mi}	R_f
147.8124	8.9125	3.3309	147.6463	8.9103	3.3539	147.1934	8.9102	3.4204	0.1
121.0933	8.8794	8.8605	120.8932	8.8546	8.8734	120.5552	8.8622	8.8436	500
Bus #7			Bus #8			Bus #9			
ψ	A_{ma}	A_{mi}	ψ	A_{ma}	A_{mi}	ψ	A_{ma}	A_{mi}	R_f
145.1755	8.9333	3.7141	143.3856	9.0448	4.0283	141.2394	9.2114	4.3684	0.1
119.0165	8.8350	8.8173	117.5816	8.8943	8.8773	115.8563	8.9981	8.9817	500

B.2. Double phase to ground and phase to phase faults

After applying the same steps, we got correct results with accuracy 100% according to fault location (maximum value of ψ at faulted bus) and fault type (within $\frac{\pi}{6} < \psi \leq \frac{\pi}{3}$). Because two types of fault double phase to ground and phase to phase fault have the same value of ψ, it is recommended to apply another feature to distinguish between them. Thus, we will use the major axis parameter for double phase. The major axis value is greater than or equals the rated voltage peak value as shown in Table 7 and 8 for ABG and AB faults. The same results for BCG, BC and ACG, AC faults are shown in Table 9-12.

TABLE 7
ELLIPSE PARAMETER RESULT FOR FAULT ABG AT BUS 5

Bus #1			Bus #2			Bus #3			
ψ	A_{ma}	A_{mi}	ψ	A_{ma}	A_{mi}	ψ	A_{ma}	A_{mi}	R_f
40.4255	7.9888	4.7794	46.4338	7.4020	3.4689	49.9952	6.9863	2.4308	0.1
19.7769	8.9599	8.9490	25.0673	8.9287	8.9154	27.9033	8.9049	8.8895	500
Bus #4			Bus #5			Bus #6			
ψ	A_{ma}	A_{mi}	ψ	A_{ma}	A_{mi}	ψ	A_{ma}	A_{mi}	R_f
54.6166	6.3961	0.8261	56.1991	6.2180	0.3126	55.3770	6.2995	0.4285	0.1
30.9328	8.8745	8.8556	31.7060	8.8679	8.8480	31.3561	8.8569	8.8372	500
Bus #7			Bus #8			Bus #9			
ψ	A_{ma}	A_{mi}	ψ	A_{ma}	A_{mi}	ψ	A_{ma}	A_{mi}	R_f
51.9627	6.5551	0.9348	49.2360	6.8302	1.4277	46.1832	7.1589	1.9469	0.1
29.7551	8.8303	8.8115	28.2688	8.8902	8.8721	26.4478	8.9946	8.9771	500

TABLE 8
ELLIPSE PARAMETER RESULT FOR FAULT AB AT BUS 5

Bus #1			Bus #2			Bus #3			
ψ	A_{ma}	A_{mi}	ψ	A_{ma}	A_{mi}	ψ	A_{ma}	A_{mi}	R_f
43.0504	9.2730	4.5214	49.0766	9.0809	3.2591	8.9856	8.9856	2.2434	0.1
19.8488	8.9697	8.9373	25.1406	8.8998	8.9396	27.9769	8.9168	8.8707	500
Bus #4			Bus #5			Bus #6			
ψ	A_{ma}	A_{mi}	ψ	A_{ma}	A_{mi}	ψ	A_{ma}	A_{mi}	R_f
57.2051	8.9017	0.6587	58.5997	8.8895	0.1495	57.9517	9.0485	0.2614	0.1
31.0055	8.8882	8.8319	31.7781	8.8823	8.8226	31.4316	8.8712	8.8122	500
Bus #7			Bus #8			Bus #9			
ψ	A_{ma}	A_{mi}	ψ	A_{ma}	A_{mi}	ψ	A_{ma}	A_{mi}	R_f
55.1435	9.2093	0.7462	52.7413	9.3572	1.2156	49.9796	9.5550	1.7011	0.1
29.8455	8.8443	8.7881	28.3725	8.9040	8.8499	26.5648	9.0083	8.9560	500

TABLE 9
ELLIPSE PARAMETER RESULT FOR FAULT BCG AT BUS 5

Bus #1			Bus #2			Bus #3			
ψ	A_{ma}	A_{mi}	ψ	A_{ma}	A_{mi}	ψ	A_{ma}	A_{mi}	R_f
160.5236	7.9848	4.7798	166.5047	7.3997	3.4685	170.0494	6.9849	2.4301	0.1
139.8108	8.9599	8.9490	145.1174	8.9287	8.9154	147.9617	8.9049	8.8895	500
Bus #4			Bus #5			Bus #6			
ψ	A_{ma}	A_{mi}	ψ	A_{ma}	A_{mi}	ψ	A_{ma}	A_{mi}	R_f
174.6802	6.3951	0.8253	176.2425	6.2158	0.3118	175.4804	6.2985	0.4258	0.1
150.9989	8.8745	8.8556	151.7738	8.8679	8.8480	151.4393	8.8569	8.8372	500
Bus #7			Bus #8			Bus #9			
ψ	A_{ma}	A_{mi}	ψ	A_{ma}	A_{mi}	ψ	A_{ma}	A_{mi}	R_f
172.3571	6.5551	0.9242	169.9406	6.8282	1.4108	167.2361	7.1519	1.9245	0.1
149.9085	8.8303	8.8115	148.4893	8.8902	8.8721	146.7433	8.9946	8.9771	500

TABLE 10
ELLIPSE PARAMETER RESULT FOR FAULT BC AT BUS 5

Bus #1			Bus #2			Bus #3			
ψ	A_{ma}	A_{mi}	ψ	A_{ma}	A_{mi}	ψ	A_{ma}	A_{mi}	R_f
163.1212	9.2682	4.5207	169.2007	9.0780	3.2578	172.7750	8.9836	2.2420	0.1
139.8647	8.9697	8.9373	145.1650	8.9396	8.8998	148.0057	8.9169	8.8707	500
Bus #4			Bus #5			Bus #6			
ψ	A_{ma}	A_{mi}	ψ	A_{ma}	A_{mi}	ψ	A_{ma}	A_{mi}	R_f
177.2446	8.9000	0.6579	178.6185	8.8855	0.1489	178.0126	9.0492	0.2587	0.1
151.0386	8.8882	8.8318	151.8122	8.8823	8.8225	151.4737	8.8712	8.8122	500
Bus #7			Bus #8			Bus #9			
ψ	A_{ma}	A_{mi}	ψ	A_{ma}	A_{mi}	ψ	A_{ma}	A_{mi}	R_f
175.4043	9.2164	0.7341	173.2147	9.3633	1.1956	170.6839	9.5574	1.6730	0.1
149.9238	8.8443	8.7881	148.4852	8.9040	8.8499	146.7158	9.0083	8.9560	500

TABLE 11
ELLIPSE PARAMETER RESULT FOR FAULT ACG AT BUS 4

Bus #1			Bus #2			Bus #3			
ψ	A_{ma}	A_{mi}	ψ	A_{ma}	A_{mi}	ψ	A_{ma}	A_{mi}	R_f
100.786	7.8882	4.4992	106.955	7.2702	3.1124	110.717	6.8340	2.0150	0.1
79.8596	8.9595	8.9493	85.1603	8.9286	8.9154	88.0036	8.9048	8.8894	500
Bus #4			Bus #5			Bus #6			
ψ	A_{ma}	A_{mi}	ψ	A_{ma}	A_{mi}	ψ	A_{ma}	A_{mi}	R_f
115.944	6.2283	0.3228	115.649	6.2632	0.3646	114.858	6.3449	0.4824	0.1
91.0417	8.8744	8.8555	90.9164	8.8684	8.8496	90.5715	8.8574	8.8388	500
Bus #7			Bus #8			Bus #9			
ψ	A_{ma}	A_{mi}	ψ	A_{ma}	A_{mi}	ψ	A_{ma}	A_{mi}	R_f
111.571	6.6042	0.9965	108.939	6.8760	1.4961	105.975	7.2005	2.0235	0.1
88.9891	8.8307	8.8131	87.5140	8.8905	8.8736	85.6971	8.9948	8.9786	500

TABLE 12
ELLIPSE PARAMETER RESULT FOR FAULT AC AT BUS 4

Bus #1			Bus #2			Bus #3			
ψ	A_{ma}	A_{mi}	ψ	A_{ma}	A_{mi}	ψ	A_{ma}	A_{mi}	R_f
103.631	9.2656	4.2319	109.8838	9.0693	2.8972	113.640	8.9755	1.8244	0.1
80.0072	8.9698	8.9371	85.2282	8.9397	8.8997	88.0622	8.8706	8.9168	500
Bus #4			Bus #5			Bus #6			
ψ	A_{ma}	A_{mi}	ψ	A_{ma}	A_{mi}	ψ	A_{ma}	A_{mi}	R_f
118.5081	8.9223	0.1537	118.2755	9.0129	0.1941	117.6447	9.1486	0.3077	0.1
91.0950	8.8882	8.8316	90.9698	8.8822	8.8259	90.6254	8.8711	8.8154	500
Bus #7			Bus #8			Bus #9			
ψ	A_{ma}	A_{mi}	ψ	A_{ma}	A_{mi}	ψ	A_{ma}	A_{mi}	R_f
114.9100	9.3146	0.7992	112.5671	9.4603	1.2743	109.8689	9.6594	1.7665	0.1
89.0470	8.8441	8.7912	87.5782	8.9037	8.8530	85.8250	9.0081	8.9589	500

C. Distributed Generation Protection

The connections of distributed generators to distribution network or a microgrid can create several protection issues. The protection of these networks using current-based protective devices is a challenging task due to the change in fault current levels directions [24]. Moreover, fault current levels in the network will aggravate the situation further .The rate of change of fault currents strongly depends on the ability of the DG to contribute to the fault current [25]. DG based induction generator does not provide a sustainable fault current during a grid disturbance. The same holds mostly for inverter-connected DG such as micro-turbines, fuel-cells and PV-systems, from which the fault current contribution can be neglected. The type of generators that might contribute a sustainable fault current is the synchronous generator [26].

New changes are adopted in the standard, which does not require disconnection from the grid during or after a fault provided that the PV generating plant should not extract more inductive reactive power than prior to fault [27]. However, such a strategy will significantly reduce the system reliability, especially when the penetration level of DGs increases. Therefore, new protection methods are required for DG connected distribution networks to improve supply reliability by using relay which is not dependent on the fault current level. By applying the protection scheme on the distribution network shown in Fig. 15, dividing this system into three zones for utility and distribution generators as shown in Fig. 19 and generating the fault feature according to the above algorithm, we conclude the following points:

- The new protection scheme is independent of fault current and DG contribution to the fault current.
- The system has different zones; and the relay at the substation communicates with the zone breakers to take appropriate actions based on maximum value of the orientation angle of ellipse as shown in Fig. 20. Fig. 21 shows the protective zones with the orientation angle during AG fault for high DG penetration. The faulted zone has the maximum angle. Fig. 14 shows the protective zones with an orientation angle AG fault without DG penetration.
- The faulted section (zone) will be isolated based on appropriate actions in the step above. Unfaulted zones are allowed to operate in an electrical island. This will increase the system reliability and prevent unnecessary customer power interruptions.

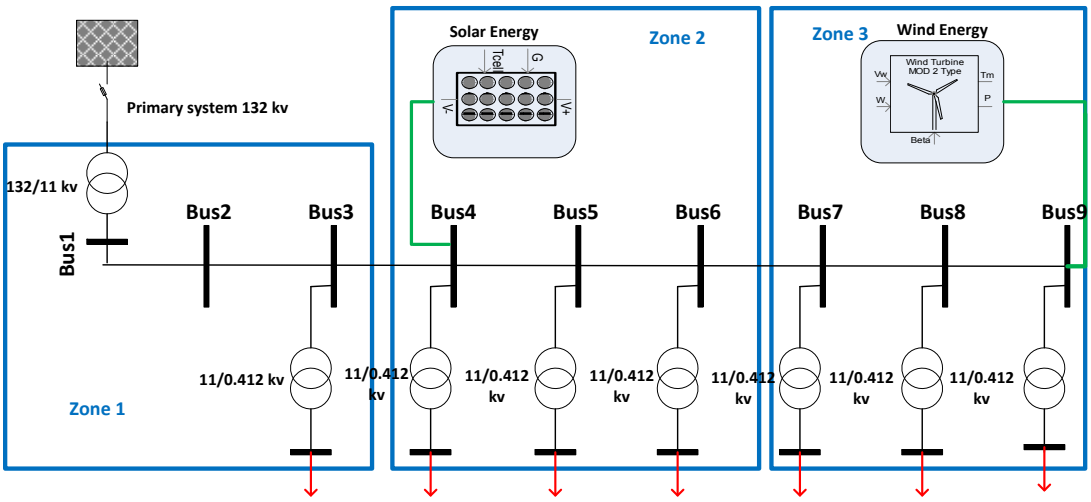

Fig. 19. Protection zones for distributed generation protection

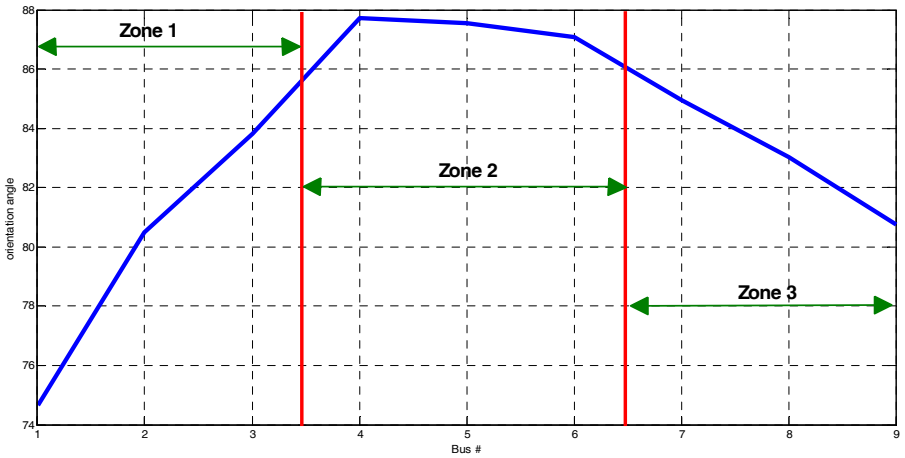

Fig. 20. Protective zones with orientation angle during AG fault for high DG penetration

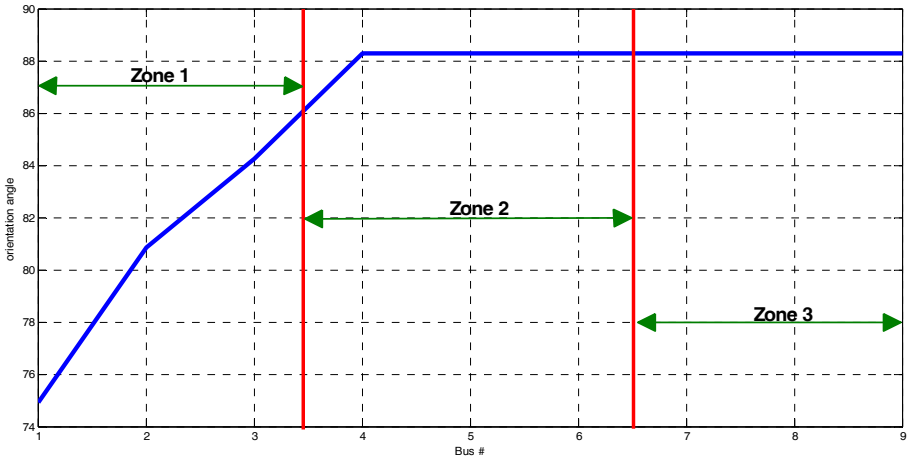

Fig. 21. Protective zones with orientation angle during AG fault without DG penetration

VI. CONCLUSIONS

This paper presented a new method to detect, classify, and localize fault types in power distribution systems based on polarization ellipse. The detection and classification process depends on unique signatures and polarization ellipse. The presented method allows dealing with distribution systems with high penetration of DG that introduces problems such as losing coordination of protection devices with consequence false tripping. This algorithm has many advantages. The fault can be detected, classified and localized within one cycle from fault incident point. This algorithm has a good result with high impedance fault. The new protection scheme which is based on the proposed algorithm is independent of fault current. DG contribution to the fault current makes a way for adaptive protection to be accepted as an alternative to conventional protection principle. It also enables the detection of cascading outages and offers mitigation approaches. In the case study, the presence of a single phase, double phase and symmetrical fault are detected; and the correct location of the fault is obtained. The proposed method has a great potential for use in real time applications.

REFERENCES

[1] M. Kezunovic, C. C. Liu, J. McDonald and L. E. Smith, "Automated fault analysis," *IEEE Tutorial*, IEEE Power Engineering Society, 2000.

[2] M. Kezunovic, I. Rikalo, "Detect and classify faults using neural nets," *IEEE Computer Applications in Power*, vol.9, no.4, pp.42-47, 1996.

[3] A. Jain, A. Thoke and R. Patel, "Fault classification of double circuit transmission line using artificial neural network," *International Journal of Electrical and Electronics Engineering*, vol. 1, no.4, pp. 230-235, 2008.

[4] A. Jain and A. Thoke, "Classification of single line to ground faults on double circuit transmission line using ANN," *International Journal of Computer and Electrical Engineering*, vol. 1, no. 2, pp. 197-203, 2009.

[5] M. Sanaye-Pasand and H. Khorashadi-Zadeh, "Transmission line fault detection and phase selection using ANN," *International Conference on Power Systems Transients*, pp. 1-6, 2003.

[6] K.S. Swarup, N. Kamaraj and R. Rajeswari, "Fault diagnosis of parallel transmission lines using wavelet based ANFIS," *International Journal of Electrical and Power Engineering*, vol. 1, no. 4, pp. 410-415, 2007.

[7] H. Zheng-you, C. Xiaoqing and F.Ling, "Wavelet entropy measure definition and its application for transmission line fault detection and identification (part II: fault detection in transmission line)," *International Conference on Power System Technology*, pp. 1-5, 2006.

[8] V. Malathi and N. Marimuthu, "Multi-class support vector machine approach for fault classification in power transmission line," *IEEE International Conference on Sustainable Energy Technologies*, pp.67-71, 2008.

[9] S. El Safty and A. El-Zonkoly, "Applying wavelet entropy principle in fault classification," *International Journal of Electrical Power & Energy Systems*, vol. 31, no. 10, pp. 604-607, 2009.

[10] J. Upendar, C. P. Gupta and G. K. Singh, "Discrete wavelet transform and genetic algorithm based fault classification of transmission systems," *National Power Systems Conference*, pp. 223-228, 2008.

[11] D. Biswarup and V. Reddy, "Fuzzy-logic-based fault classification scheme for digital distance protection," *IEEE Transactions on Power Delivery*, vol. 20, no. 1, pp. 609-616, 2005.

[12] K. Razi, M. Hagh and G. Ahrabian, "High accurate fault classification of power transmission lines using fuzzy logic," *International Power Engineering Conference*, pp. 42-46, 2007.

[13] S. Vaslilc and M. kezunovic, "Fuzzy ART neural network algorithm for classifying the power system faults," *IEEE Transactions on Power Delivery*, vol. 20, no. 2, pp. 1306-1314, 2005.

[14] S. Samantaray, P. Dash and G. Panda, "Transmission line fault detection using time-frequency analysis," *IEEE INDICON Conference*, pp. 162-166, 2005.

[15] E. Styvaktakis, M. Bollen and I. Gu, "Automatic classification of power system events using rms voltage measurements," *IEEE Power Engineering Society Summer Meeting*, pp. 824-829, 2002,

[16] H. Saadat, *Power System analysis*, McGraw Hill, 2002.

[17] P. J. Schreier, "Polarization ellipse analysis of nonstationary random signals," *IEEE Transactions on Signal Processing*, vol. 56, no. 9, pp. 4330-4339, 2008.

[18] Y. Yang, R. Tao and Y. Wang, "A new SINR equation based on the polarization ellipse parameters," *IEEE Transactions on Antennas and Propagation*, vol. 53, no. 4, pp. 1571-1577, 2005.

[19] E. Collett, *Polarized Light in Fiber Optics*, Polawave Group, 2003.

[20] J. V. Olson and R. Domke, "Instrument to measure the polarization state of waves," *Review of Scientific Instruments*, vol. 56, no. 2, pp. 278-282, 1985.

[21] Y. Xia, D. P. Mandic, "Widely linear adaptive frequency estimation of unbalanced three-phase power systems," *IEEE Transactions on Instrumentation and Measurement*, vol. 61, no. 1, pp. 74-83, 2012.

[22] O. A. Saraereh, Q. Alsafasfeh, A. Al-Tarabsheh, A. Arfoa and I. Etier, "Least squares fitting based fault classification in distribution systems," *Journal of Energy and Power Engineering*, vol. 4, no. 8, pp. 560-567, 2014.

[23] M. A. Ibrahim, *Disturbance Analysis for Power Systems*, John wiley, 2012.

[24] M. Dewadasa, A. Ghosh, G. Ledwich and M. Wishart, "Fault isolation in distributed generation connected distribution networks," *IET Generation, Transmission and Distribution*, vol. 5, no. 10, pp. 1053-1061, 2011.

[25] N. Jenkins, R. Allen, P. Crossley, D. Kirschen and G. Strbac. *Embedded Generation (Power and Energy Series 31)*. LAVOISIER S.A.S., 2000.

[26] IEEE Std. 1547–2003 "*IEEE standard for interconnecting distributed resources with electric power systems*," 2003.

[27] A. M. El-Zonkoly, "Fault diagnosis in distribution networks with distributed generation," *Smart Grid and Renewable Energy*, vol. 2, no. 1, pp. 1-11, 2011.